JOURNAL OF MATERIALS SCIENCE 23 (1988) 3485–3489

# X-ray diffraction study of an amorphous $Al_{60}Ge_{30}Ni_{10}$ alloy

E. MATSUBARA, K. HARADA, Y. WASEDA
*The Research Institute of Mineral Dressing and Metallurgy (SENKEN), Tohoku University, Sendai 980, Japan*

A. INOUE, Y. BIZEN, T. MASUMOTO
*Institute for Materials Research, Tohoku University, Sendai 980, Japan*

The ordinary X-ray diffraction profile and anomalous X-ray scattering profiles at nickel and germanium $K$ absorption edges of amorphous $Al_{60}Ge_{30}Ni_{10}$ alloy have been determined. The results indicate the characteristic feature of the coexistence of nickel-rich highly ordered crystal-like regions and germanium-rich amorphous regions. From the environmental radial distribution function around germanium atoms, the coordination number around a germanium atom is estimated at about 4. Thus, an amorphous germanium-like structure may be quite feasible in this region.

## 1. Introduction

Studies on numerous aluminium-base amorphous alloys (see e.g. [1]) are vigorously proceeding in order to search for new aluminium-base materials whose physical or chemical properties are superior to those of known aluminium-base crystalline alloys. Recently, ternary Al–Ge–Ni alloys have been found to produce a non-crystalline phase over a wide range of concentration by rapid quenching, and some of them show good ductility [2], suggesting enough potential for future use. Some interesting features were reported for these alloys [2]; for example, a split first peak in the X-ray diffraction pattern of $Al_{60}Ge_{30}Ni_{10}$ alloy is found, and a modulated pattern is also observed in the bright-field image by transmission electron microscopy. The split first peak in the amorphous ternary alloy has also been interpreted by the coexistence of the two components of aluminium-rich and germanium-rich amorphous phases inferred from previous results on amorphous $Pt_{60}Pb_{20}Sb_{20}$ [3] and $Au_{55}Pb_{22.5}Sb_{22.5}$ [4], in which a split first peak of the X-ray diffraction profile was detected and ascribed to the coexistence of platinum- or gold-rich and lead-rich amorphous phases [4]. However, their atomic structure has not yet been revealed. Thus, additional structural information on amorphous Al–Ge–Ni alloys is strongly desired for a better understanding of their characteristic features.

The main purpose of this work is to present the further structural analysis of an amorphous $Al_{60}Ge_{30}Ni_{10}$ alloy by ordinary X-ray diffraction and by anomalous X-ray scattering (AXS) techniques.

## 2. Experimental procedure

An ingot of the alloy composed of 60 at % Al, 30 at % Ge and 10 at % Ni nominal composition was prepared by arc-melting a mixture of pure aluminium (99.99 wt %), germanium (99.99 wt %) and nickel (99.8 wt %) in a purified argon atmosphere. From the master ingot, ribbons about 1 mm wide and 0.017 mm thick were prepared by a single-roller melt-spinning technique. Since this ternary sample was very brittle and the ribbon was obtained as small pieces, for X-ray measurements these short pieces of ribbon were closely arranged on aluminium frames about 15 mm wide and 10 mm high, and a few layers of the sample were placed upon them.

An ordinary X-ray diffraction profile was obtained using an $\omega$–$2\theta$ diffractometer with a molybdenum X-ray tube, and a singly bent pyrolytic graphite monochromator in the diffracted beam. The scattering intensity from the sample was measured by a scintillation detector with a pulse-height analyser for the reduction of background noise. The intensity profile was obtained from 7 to 153 $nm^{-1}$ for the wave-vector $Q = 4\pi \sin\theta/\lambda$, where $\theta$ is half the angle between incident and diffracted beams and $\lambda$ is the wavelength. In order to obtain the same counting statistics for every measured point, a fixed-count mode was used to collect at least 20 000 counts.

The absorption, polarization, and Compton scattering were corrected for [5, 6], and the measured intensities were converted into electron units per atom by the generalized Krogh-Moe–Norman method [7], using the atomic scattering factors and anomalous dispersion corrections tabulated in the International Tables [8]. The total structure factor $S(Q)$ was evaluated from the coherent scattering intensity in absolute units $I_{eu}^{coh}(Q)$ by the equation [5, 6]

$$S(Q) = \frac{I_{eu}^{coh}(Q) - \langle f^2 \rangle + \langle f \rangle^2}{\langle f \rangle^2} \quad (1)$$

where $\langle f \rangle$ is the average atomic scattering factor and $\langle f^2 \rangle$ is the mean square of the atomic scattering factors. The radial distribution function (RDF) was obtained by the Fourier transformation of $S(Q)$. That

0022–2461/88 $03.00 + .12 

is,

$$4\pi r^2\varrho(r) = 4\pi r^2\varrho_0 + \frac{2r}{\pi}\int_0^\infty Q[S(Q) - 1]\sin(Qr)\,dQ \quad (2)$$

where $\varrho(r)$ is the total radial density function and $\varrho_0$ is the average number density of the sample.

The measurements were carried out with synchrotron radiation at the Photon Factory of the National Laboratory for High Energy Physics, Tsukuba, Japan. Monochromatic incident beams at any energy from 4 to 20 keV were obtained with a silicon 1 1 1 double-crystal monochromator. The sample was mounted on a vertical diffractometer. The intensity of the incident beam was monitored by an $N_2$ gas-flow type ion chamber placed in front of the sample. By adopting a fixed monitor-count mode, the total number of photons to the sample was kept constant for all measurements. The diffracted intensities were measured by a portable pure germanium solid-state detector so that the coherent intensity (including the structural information) and $K\alpha$ fluorescent radiation from the sample were measured separately [9]. The $K\beta$ fluorescence overlapping with the coherent radiation near the absorption edge was numerically estimated from the measured $K\alpha$ radiation and tabulated $K\alpha$ to $K\beta$ ratio [10], and eliminated from the coherent intensity. Then, the coherent intensity was corrected for the absorption by the sample and air in the beam path and for the efficiency of the ion chamber at the incident beam energy, and converted into absolute units using the generalized Krogh-Moe-Norman method [7]. Then the Compton scattering intensity was corrected by subtracting the theoretical values given by Hajdu [11]. Details of the experimental setting used for AXS measurements at the Photon Factory are explained elsewhere [12].

In the present measurements, only the energies on the lower-energy side of the nickel and germanium $K$ absorption edges were used for the AXS measurements because of particular near-edge phenomena, for example XANES (X-ray Absorption Near Edge Structure), EXAFS (Extended X-ray Absorption Fine Structure) and extremely intense fluorescent radiation on the higher-energy side of the edge. For AXS measurement it is crucial to set the incident beam at an exact energy near the edge in order to carry out the measurement successfully. In the present work, this has been accomplished by determining the energy dependence of the values $f'$ of the element estimated from the integrated intensities of its powder peaks around its absorption edge, and comparing them with the theoretical values calculated by the method of Cromer and Lieberman [13]. Since the details of the basic concepts of the AXS technique have been explained elsewhere [14], only basic equations necessary for the AXS analysis will be given below.

When the energy of the incident beam is tuned to the vicinity of an absorption edge of a specific element A, the detected variation in intensity is attributed only to the change of the real and imaginary parts of the anomalous dispersion terms $f'$ and $f''$ of the A element, respectively. Since the variation of the term $f''$ is small and almost constant on the lower-energy side of the edge, the difference between the scattering intensities measured at two energies $E_1$ and $E_2$ ($E_1 > E_2$) on the lower-energy side of the absorption edge is given in a ternary case by

$$\begin{aligned}\Delta I_A(Q) &= I(Q, E_2) - I(Q, E_1) \\ &= c_A[f'_A(E_2) - f'_A(E_1)] \\ &\quad \times \int_0^\infty 4\pi r^2 \sum_{j=1}^{3}\{\mathrm{Re}[f_j(Q, E_1) + f_j(Q, E_2)] \\ &\quad \times [\varrho_{Aj}(r) - \varrho_{0j}]\}\frac{\sin(Qr)}{Qr}\,dr \end{aligned} \quad (3)$$

where $c_A$ is the atomic fraction of the A element. The Fourier transformation of the quantity $\Delta I_A(Q)$ gives the environmental RDF corresponding to the local environmental structure around an A atom; that is,

$$4\pi r^2\varrho_A(r) = 4\pi r^2\varrho_0 + \frac{2r}{\pi}\int_0^\infty \frac{Q\Delta I_A(Q)\sin(Qr)}{c_A[f'_A(E_2) - f'_A(E_1)]\,W(Q)}\,dQ \quad (4)$$

$$W(Q) = \sum_{j=1}^{3} c_j[f_j(Q, E_1) + f_j(Q, E_2)] \quad (5)$$

For example, for the ternary system, six partial RDFs are known to overlap each other in the ordinary RDF, but the environmental RDF defined in Equation 4 is a sum of three AA, AB, AC partial RDFs. Thus, the environmental RDF can provide a more local atomic structure about a specific element, without complete separation of all partial RDFs. This energy-derivative method of the AXS along the line of Shevchik's scheme [15, 16] was first used by Fuoss *et al.* [17] with synchrotron radiation under the name of differential anomalous scattering (DAS) and the differential distribution function (DDF).

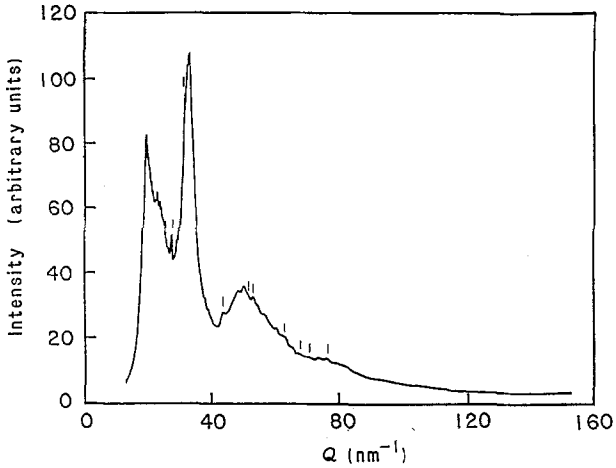


*Figure 1* X-ray diffraction profile tor amorphous $Al_{60}Ge_{30}Ni_{10}$ alloy. Small bars indicate peak positions of polycrystalline aluminium metal.

## 3. Results and discussion

Fig. 1 shows an intensity profile of the sample by Mo$K\alpha$ radiation. Two sharp characteristic peaks at 19 and 33 $nm^{-1}$, followed by a third peak with a shoulder at about 50 $nm^{-1}$, and a small and diffuse fourth peak at about 80 $nm^{-1}$ are observed. The general profile of the intensity pattern can be classified into the similar one commonly observed in amorphous alloys, except for the split of the main peak. In

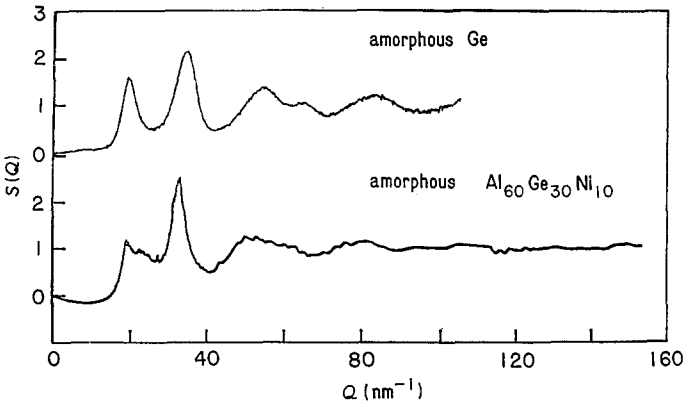


*Figure 2* Total structure factors $S(Q)$ for amorphous $Al_{60}Ge_{30}Ni_{10}$ in the present work and for amorphous germanium reported by Kortright [20].

Fig. 1, it is also noted that there are many "spikes" overlapping the diffuse profile. These small spikes perhaps indicate that there is an extremely small amount of crystallized regions in the sample. We tried to identify them by comparing the peak positions with known compounds formed by some combinations of nickel, aluminium or germanium. As a result, it was found that some of them are explained by aluminium whose peaks are marked by short bars in Fig. 1. Other spikes have not been explained by known equilibrium compounds. It is more likely that they might result from metastable phases since there are some reports of metastable phases in liquid-quenched aluminium alloys [18, 19]. Incidentally, it was confirmed that the RDF obtained from Fourier transformation of the intensity profile with manual removal of these sharp small spikes does not show any significant difference from the RDF determined from the original profile in the figure.

In Fig. 2, the structure factor $S(Q)$ of the sample is shown with that of amorphous germanium from Kortright [20]. It is seen immediately that the basic profiles of $S(Q)$ are similar to each other in peak positions and values, etc. Thus, it is imagined that the structure of the sample might be similar to the structure of amorphous germanium. In order to obtain further insights into the characteristic structure of this amorphous $Al_{60}Ge_{30}Ni_{10}$ alloy, the AXS technique was applied to the sample at the nickel and germanium $K$ absorption edges. The energies used for the measurements were 8.3067 and 8.0316 keV for the nickel $K$ edge, and 11.0795 and 10.8047 keV for the germanium $K$ edge. Incidentally, these energies correspond to energies 25 and 300 eV below each edge. The profiles observed at the two energies for nickel and germanium edges are shown in Figs 3 and 4, respectively. The differential intensity profiles of the intensity curves are given in the top of each figure. From these two differential intensity profiles, it is promptly noted that their basic patterns appear completely different. At the nickel edge, the differential intensity profile consists of several discrete peaks like those from crystals, and their values are both positive and negative. On the other hand, the differential intensity profile at the germanium $K$ edge shows a diffuse non-crystalline pattern overlapping with small spikes.

Here, let us consider the effect of $f'$ on the total coherent intensity in various structures, before proceeding to a discussion of the relation between the differential intensity profiles and atomic structure. In order to simplify the explanation, a binary alloy AB is considered. If A and B atoms are arranged at random in the crystal, its structure factor is proportional to the average atomic scattering factor, i.e. $(c_A f_A + c_B f_B)$, where $c_A$ and $c_B$ are the atomic fractions of A and B, and $f_A$ and $f_B$ are the atomic scattering factors of A and B. Thus, a decrease in the quantity $f_A$ near the absorption edge due to the decrease in the quantity of the real part of the anomalous dispersion term results in a decrease in the scattering intensity. Consequently, the differential intensity defined by Equation 3 is positive for all differential peaks. Similarly, in an amorphous alloy, where all constituent elements are distributed at random, the resultant differential intensity profile should be positive. However, if a crystal has an ordered structure, all differential peaks may not be positive. The reason is as follows. Let us consider the AXS measurement at the absorption edge for the A element. The structure factor at some of the superlattice points should include the term $(f_B - f_A)$. Therefore, the scattering intensities at such peaks increase near the absorption edge of the element A. As a result, the differential intensity profile in the ordered structure consists of a mixture of positive and negative peaks.

The differential intensity profile at the nickel edge in Fig. 3 corresponds to this latter example. Namely, it is

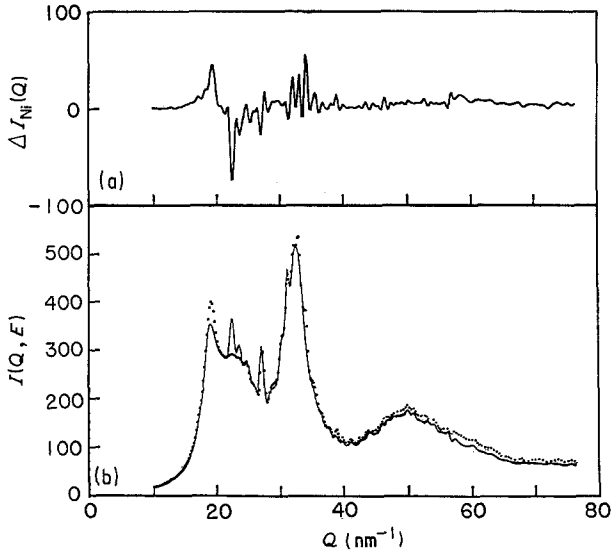


*Figure 3* (a) Differential intensity profile of amorphous $Al_{60}Ge_{30}Ni_{10}$ alloy obtained from (b) intensity data sets measured at photon energies (——) 8.3067 keV and (···) 8.0316 keV; these are 25 and 300 eV below the nickel $K$ absorption edge, respectively.

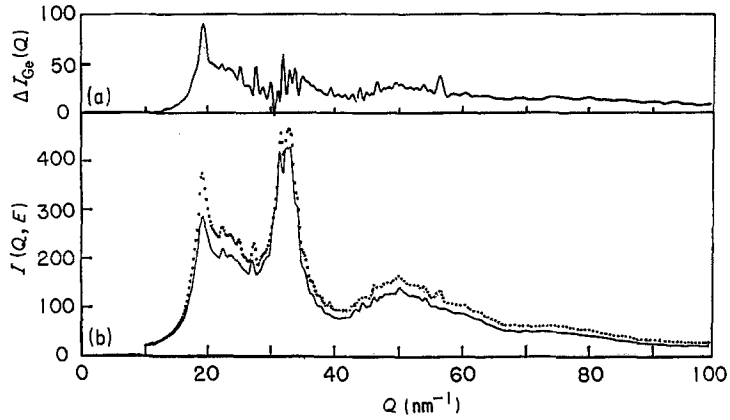


*Figure 4* (a) Differential intensity profile of amorphous $Al_{60}Ge_{30}Ni_{10}$ alloy obtained from (b) intensity data sets measured at photon energies (——) 11.0795 keV and (···) 10.8047 keV; these are 25 and 300 eV below the germanium $K$ absorption edge, respectively.

imagined that most of nickel atoms in the sample are present in a crystal-like region and form a highly ordered structure with aluminium or germanium atoms, although a definite structure of this crystal-like region cannot be obtained from the present results alone. On the other hand, the differential intensity profile at the germanium edge in Fig. 4 clearly indicates a non-crystalline pattern similar to the original one, although the relative intensity of the second peak drops drastically in comparison with that of the first. This implies that most of the germanium atoms are contained in the non-crystalline region. The structure of this non-crystalline region can be estimated from the environmental RDF in Fig. 5. In this figure, the RDF of amorphous germanium [20] is also shown. It is readily noted that the environmental RDF at the germanium $K$ edge resembles the RDF of the amorphous germanium, and the coordination number was estimated to be 4.1 from the area of the first peak. Thus, it is plausible that the atomic arrangements around a germanium atom is extremely similar to those in amorphous germanium. The small spikes overlapping with the diffuse profile indicated in Fig. 1 may be understood as due to Ge–Ni pairs strongly correlated in the ordered phase. For a further quantitative description of the characteristic structure of an amorphous $Al_{60}Ge_{30}Ni_{10}$ alloy, an additional structural analysis for detecting a finer profile change is required at each edge, particularly at the nickel edge. It must be the first consideration to identify the peaks obtained in the differential intensity profile at the nickel edge, and to attempt a quantitative explanation of the intensity changes of these peaks. Such AXS measurements are under consideration. However, it may be concluded from the present results that the modulated region observed in the transmission electron microscope [2] corresponds to harmony between the non-crystalline regions consisting of mainly germanium and aluminium whose local structure around germanium is close to that of the amorphous germanium, and highly ordered crystal-like regions mainly related to the nickel atom correlations.

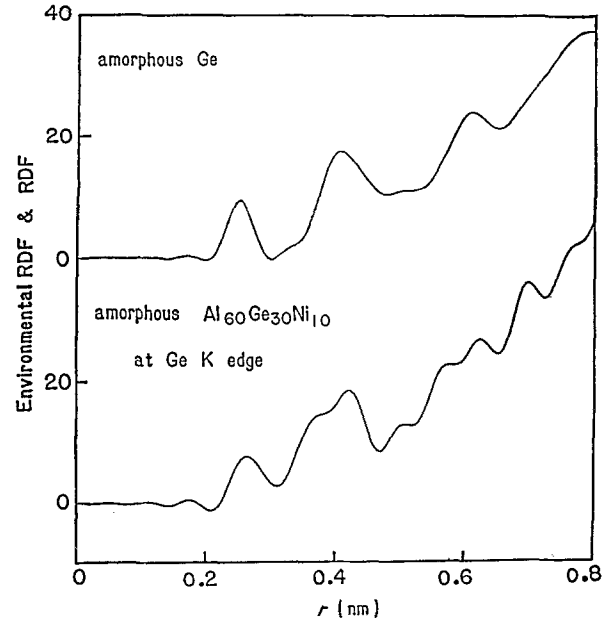


*Figure 5* Environmental RDF obtained from Fourier transformation of the differential intensity profile in Fig. 4 of amorphous $Al_{60}Ge_{30}Ni_{10}$ alloy below the germanium $K$ absorption edge, and the radial distribution function (RDF) of amorphous germanium reported by Kortright [20].


## Acknowledgements

A part of this research was supported by the Mitsubishi Foundation for a research project on anomalous X-ray scattering in 1986. E.M. and Y.W. particularly want to thank the staff of the Photon Factory, National Laboratory for High Energy Physics, Drs T. Ishikawa and M. Nomura and Professors T. Matsushita, H. Iwasaki and M. Ando.


## References


1. C. SURYANARAXANA, "Rapidly Quenched Metals, A Bibliograpy" (IFI/Plenum Data, New York, 1980).
2. A. INOUE, M. YAMAMOTO, H. M. KIMURA and T. MASUMOTO, *J. Mater. Sci. Lett.* **6** (1987) 194.
3. A. R. YAVERI and P. DESRE, *ibid.* **5** (1986) 509.
4. M. C. LEE, J. M. KENDALL and W. L. JOHNSON, *Appl. Phys. Lett.* **40** (1982) 382.
5. C. N. J. WAGNER, *J. Non-Cryst. Solids* **31** (1978) 1.
6. Y. WASEDA, "The structure of Non-Crystalline Materials", (McGraw-Hill, New York, 1980) p. 26.
7. C. N. J. WAGNER, H. OCKEN and M. L. JOSHI, *Z. Naturforsch.* **20a** (1965) 325.
8. International Tables for X-ray Crystallography, Vol. IV (Kynoch, Birmingham, 1974) p. 148.
9. S. AUR, D. KOFALT, Y. WASEDA, T. EGAMI, R. WANG, H. S. CHEN and B. K. TEO, *Solid State Commun.* **48** (1983) 111.
10. N. VENKATESWARA RAO, S. BHULOKA REDDY, G. SATYANARAYANA and D. L. SASTRY, *Physica* **138c** (1986) 215.
11. F. HAJDU, *Acta Crystallogr.* **A27** (1971) 73.
12. Y. WASEDA, E. MATSUBARA and K. SUGIYAMA, *Sci. Rep. RITU* **34A** (1988) 1.

13. D. T. CROMER and D. LIEBERMAN, *J. Chem. Phys.* **53** (1970) 1891.
14. Y. WASEDA, "Novel Application of Anomalous X-ray Scattering for Structural Characterization of Disordered Materials" (Springer, Heidelberg, 1984) p. 47.
15. N. J. SHEVCHIK, *Phil. Mag.* **35** (1977) 805.
16. *Idem, ibid.* **35** (1977) 1289.
17. P. H. FUOSS, P. EISENBERGER, W. K. WARBURTON and A. BIENENSTOCK, *Phys. Rev. Lett.* **46** (1981) 1537.
18. U. KOSTER, *Z. Metalkde* **63** (1972) 472.
19. *Idem, Acta Metall.* **20** (1972) 1361.
20. J. B. KORTRIGHT, PhD thesis, Stanford University, SSRL Report 84/05 (1984) p. 81.

*Received 26 October 1987*
*and accepted 23 February 1988*